Recent Progress in Terahertz Quantum Cascade Lasers

Sushil Kumar

(Invited Paper)

***Abstract*—Terahertz quantum cascade lasers (QCLs) emit radiation due to intersubband optical transitions in semiconductor superlattices that could be engineered by design. Among a variety of possible design schemes, we have pursued designs that utilize strong electron–phonon interaction in the semiconductor as a means to establish population inversion for optical gain. This report describes the recent progress in *phonon-depopulated* terahertz QCLs. Operation above 160 K has been realized in GaAs/AlGaAs-based QCLs with *metal–metal* waveguides for frequencies ranging from 1.8–4.4 THz ($\lambda \sim 170$–$70\ \mu$m). A record highest operating temperature of 186 K has been demonstrated for a 3.9-THz QCL based on a *diagonal* design scheme. Also, operation down to a frequency of 1.45 THz ($\lambda \sim 205\ \mu$m) has been achieved. Whereas metal–metal waveguides provide strong mode confinement and low loss at terahertz frequencies, obtaining single-mode operation in a narrow beam-pattern-posed unconventional challenges due to the subwavelength dimensions of the emitting aperture. New techniques in waveguide engineering have been developed to overcome those challenges. Finally, a unique method to tune the resonant-cavity mode of metal–metal terahertz "wire lasers" has been demonstrated to realize continuous tuning over a range of 137 GHz for a 3.8-THz QCL.**

***Index Terms*—Distributed feedback, far-infrared, intersubband laser, quantum cascade laser, resonant phonon, surface-emitting laser, terahertz (THz), tunable laser.**

I. Introduction

THE TERAHERTZ region of the electromagnetic spectrum ($\nu \sim 0.5$–10 THz, $\lambda \sim 600$–$30\ \mu$m, $\hbar\omega \sim 2$–40 meV) has remained underdeveloped in large part due to lack of suitable techniques to generate coherent high-power radiation. Many molecules and solids have strong and distinct spectral signatures at terahertz frequencies, which makes terahertz technology important for both science and commercial applications related to spectroscopy and imaging [1]. Some potentially important applications include remote sensing of earth's atmosphere, and in astronomy to understand the formation of planets, stars, and galaxies [2]. This is because terahertz optical transitions are readily thermally excited due to their low energies making them ideal for passive emission spectroscopy. For imaging applications [3], terahertz radiation is useful for security-related detection of weapons, drugs, and explosives, since many materials such as paper, plastics, and ceramics, which are opaque to visible frequencies, are transmissive at longer wavelengths. In comparison to microwaves, terahertz radiation provides a better spatial resolution due to its shorter wavelength. When compared to imaging with the high-energy X-rays, terahertz imaging is noninvasive and can provide much better contrast in terms of identification of different materials due to their largely different absorption and refraction indexes across the terahertz spectrum. For similar reasons, terahertz imaging can find potential applications in biology and medicine [4], in areas as diverse as cancer research, label-free DNA sensing, and nondestructive evaluation of pharmaceutical products. All of the aforementioned applications will benefit from compact high-power (tens of milliwatt) coherent sources of radiation to enable imaging in real time, and sensing with array detectors operating at room temperature.

There has been a spur of research activities in terms of technology development to advance the field of terahertz science [6], [7], of which, the advent of a terahertz semiconductor *quantum cascade* laser (QCL) [5] carries particular importance. Terahertz QCLs are arguably the only solid-state terahertz sources that can deliver average optical power levels much greater than milliwatt that is essential for imaging applications, and also continuous wave (CW) operation for the frequency stability desired in high-resolution spectroscopy techniques. Terahertz QCLs have witnessed rapid development since their first demonstration in 2002 with a frequency coverage from 1.2 to 5 THz (when operated without the assistance of an external magnetic field) [8]–[10]. A wide variety of active-region designs have been published [5], [11]–[20]. Whereas the initial demonstration of terahertz QCLs was done with the aid of a single-plasmon waveguiding scheme [5], the subsequent development of double-plasmon metal–metal waveguides [21] has led to higher operating temperatures in both pulsed (186 K) [22] and CW (117 K) [23], [24] operation. Due to the subwavelength dimensions of the emitting aperture in the metal–metal waveguides, their emission is characterized by divergent beam patterns and low output powers [25], [26]; however, unique distributed-feedback (DFB) techniques have recently been demonstrated to achieve single-mode operation with narrow beam patterns [27]–[31]. Fig. 1 summarizes some of the important developments in terahertz QCLs chronologically in the relatively short span of eight years as mentioned earlier.

Manuscript received March 22, 2010; revised April 24, 2010; accepted April 27, 2010. Date of publication June 21, 2010; date of current version February 4, 2011. This work was supported by the Air Force Office of Scientific Research, by the National Aeronautics and Space Administration, and by the National Science Foundation. The work was performed in part at the U.S. Department of Energy, Center for Integrated Nanotechnologies, and Sandia National Laboratories under Contract DE-AC04-94AL85000.

The author is with the Research Laboratory of Electronics, Massachusetts Institute of Technology, Cambridge, MA 02139 USA (e-mail: sushil@mit.edu).

Color versions of one or more of the figures in this paper are available online at http://ieeexplore.ieee.org.

Digital Object Identifier 10.1109/JSTQE.2010.2049735

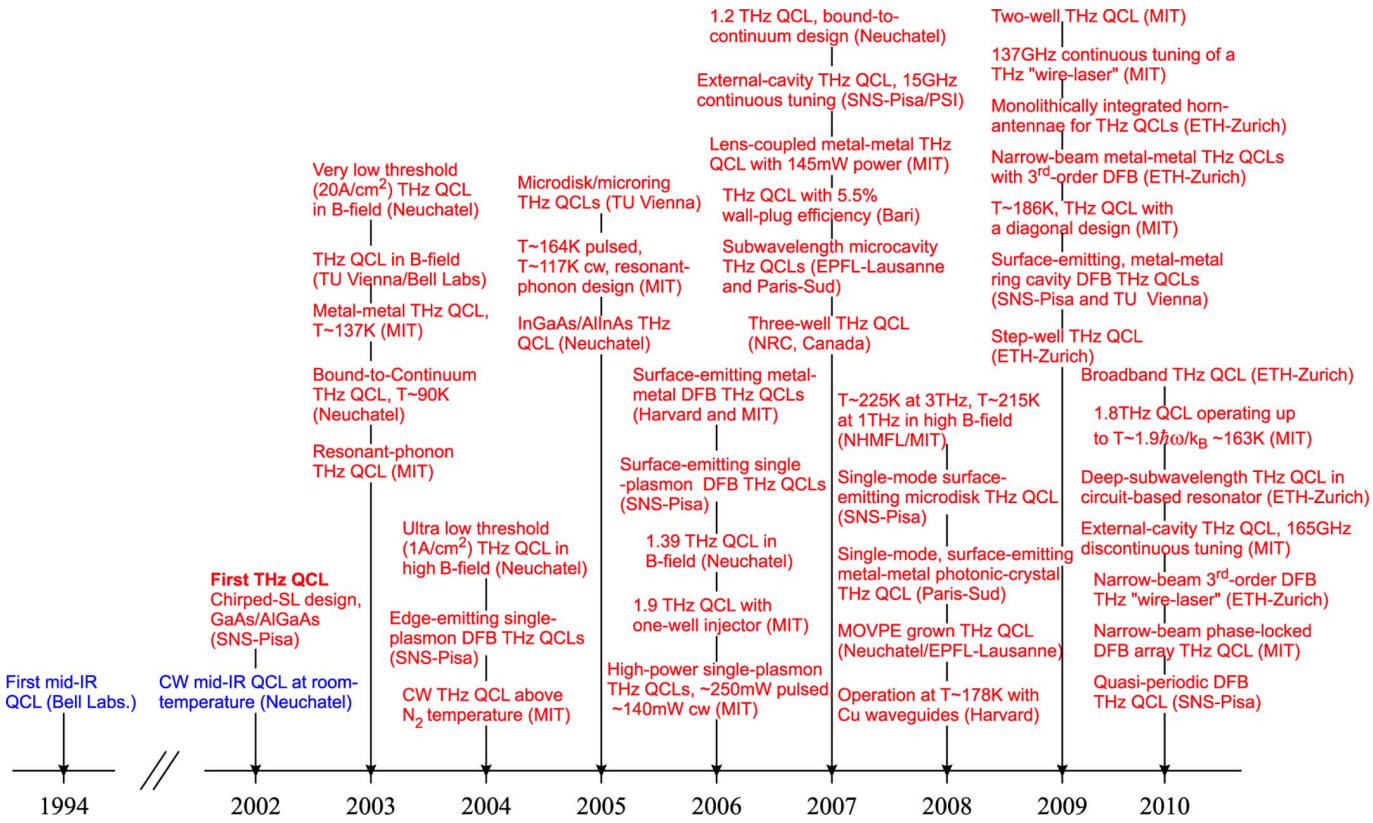

Fig. 1. Chronological list of important developments related to QCLs since their advent in 2002 [5]. Theoretical and experimental research related to study of optoelectronic characteristics of terahertz QCLs, and also experimental research in applied areas is not included for brevity.

With recent demonstrations of real-time imaging using terahertz QCLs [32], their phase locking to microwave-frequency-reference oscillators [33], [34], and also techniques for frequency tunability in the range of ∼100 GHz [35], [36], it may be argued that QCL technology now meets all the expectations required from terahertz radiation sources for the targeted applications in spectroscopy, imaging, and remote sensing. However, the requirement for cryogenic cooling is an impediment toward their viability and cost-effectiveness, and therefore, improvement of their operating temperatures is the single most important research goal in the field. The best performing terahertz QCLs in terms of temperature employ the fast electron-longitudinal-optical-phonon (electron-LO-phonon) scattering in the semiconductor as a means to establish a population inversion for optical gain. Operation above 160 K has now been demonstrated in frequencies ranging from 1.80–4.4 THz [20], [22], [37], [38] from such designs. This report summarizes some of the key recent results for phonon-depopulated terahertz QCLs including aspects related to the active-region design, properties of metal–metal waveguides, and some unconventional techniques to realize single-mode operation with narrow beam patterns and also continuous tunability of single-mode lasing behavior in such waveguides.

II. Terahertz QCL Active Region

Till date [20], terahertz QCLs have utilized resonant tunneling (RT) [40], [41] as a means to inject carriers (electrons) into the upper laser subband. The focus of our study has been the designs that utilize the fast electron-LO-phonon scattering in the semiconductor for depopulation of the lower laser subband to establish a population inversion [11]. The simplest terahertz QCL design with RT injection and phonon-mediated depopulation is three-level structure, as shown in Fig. 2 [42]. By means of this simple design, we will now elucidate the working principle of a terahertz QCL and its electrical behavior as a function of externally applied static electric-bias field. Carriers traverse through the quantum cascade structure in the growth direction by the mechanism of tunneling. The tunneling probability is enhanced for a bias at which two subbands across a potential barrier are at the same energy, which then makes the tunneling a resonant process. For example, in the three-level terahertz QCL design shown in Fig. 2, two such resonance conditions correspond to the $1'$–2 and $1'$–3 alignments at 10 and 14 kV/cm, respectively. A numerical computation [39] of the current density and population inversion between the radiative subbands (Δn_{32}) shows the working principle. A positive population inversion (leading to optical gain) is established in the structure upon preferential injection of carriers into the upper subband 3, which occurs when the structure is biased past the $1'$–2 alignment. QCLs with RT injection could effectively be reduced to a three-level scheme as shown, in which case, an essential design requirement is to have the current density at the $1'$–3 alignment ($J_{1'3}$) be larger than that at the $1'$–2 alignment ($J_{1'2}$, the so-called parasitic leakage current density that artificially enhances the lasing threshold

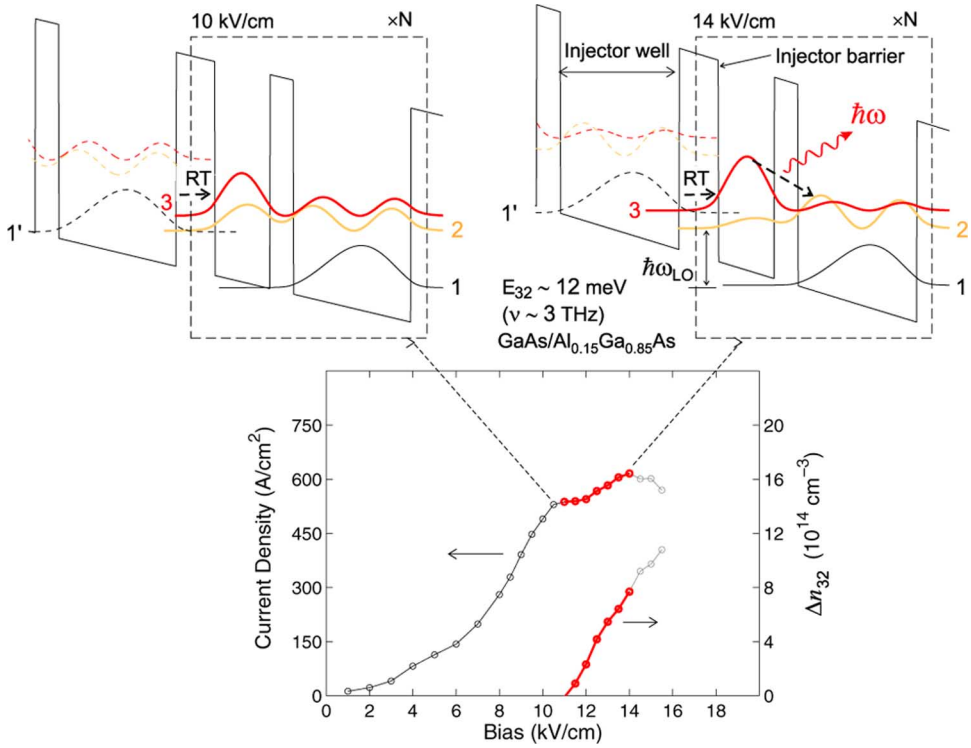

Fig. 2. Numerically computed current density and population inversion Δn_{32} (which is proportional to the intersubband gain), for an example, three-level terahertz QCL design as a function of externally applied electrical bias field for a lattice temperature of 25 K. The results were computed using an ensemble Monte Carlo simulation that accounted for the intramodule scattering mechanisms semiclassically and treated RT transport within a density matrix formalism [39]. The radiative transition is from $3 \rightarrow 2$ corresponding to a frequency of 3 THz ($\hbar\omega \sim E_{32} \sim 12$ meV), and 1 is the injector subband. For the shown design, the injector anticrossing $2\hbar\Omega_{1'3} \sim 2$ meV, radiative oscillator strength $f_{32} \sim 0.6$, and average doping 5×10^{15} cm^{-3}. Electrons are injected into the upper radiative subband 3 from $1'$ by the mechanism of RT and are depopulated from lower subband 2 by fast electron–phonon scattering, where $E_{21} \approx \hbar\omega_{\mathrm{LO}}$ is resonant with the optical phonon energy (~ 36 meV in GaAs). Optimum injection (i.e., the bias for the maximum of the current density) occurs at the $1'$–3 alignment bias field. The curves are highlighted in red (thick lines) for the "usable" bias region in which the gain is positive prior to occurrence of NDR in the *I–V* characteristics.

current density of terahertz QCLs [43]). This guarantees positive differential resistance in the superlattice's *I–V* characteristics in the bias regime with positive gain such that electrical instabilities corresponding to a negative differential resistance (NDR) could be avoided [44], an essential feature of the injector region in the QCLs [45]. Approximating unity injection efficiencies at the corresponding resonance conditions and neglecting radiative transport, estimates of current densities could be calculated analytically from the following expressions [46]:

$$J_{1'3} = e\, n_{2\mathrm{D}} \left(\frac{2\,\Omega_{1'3}^2 \tau_{\|}}{4\,\Omega_{1'3}^2 \tau_{\|} \tau_3 [1 + \tau_{21}/(2\tau_{32})] + 1} \right) \quad (1)$$

$$J_{1'2} = e\, n_{2\mathrm{D}} \left(\frac{2\,\Omega_{1'2}^2 \tau_{\|}}{4\,\Omega_{1'3}^2 \tau_{\|} \tau_{21} + 1} \right) \quad (2)$$

where $n_{2\mathrm{D}}$ is the 2-D doping density in the QCL structure, $2\hbar\Omega_{mn}$ is the energy splitting at the anticrossing of subbands m and n (which, apart from the shape of the tight-binding wavefunctions, relates exponentially to the thickness of the potential barrier), τ_{ij} is the nonradiative scattering time from subband $i \rightarrow j$, $\tau_3 \equiv (\tau_{31}\tau_{32})/(\tau_{31} + \tau_{32})$, and $\tau_{\|}$ is the dephasing time for the tunneling process [39].

Assuming a Lorentzian lineshape for the $3 \rightarrow 2$ radiative transition with a full-width half-maximum linewidth of $\Delta\nu$, the expression for the peak intersubband gain (per unit length) is

$$g = \frac{e^2}{2\pi m^* \epsilon_0 n_{\mathrm{r}} c} \frac{\Delta n_{32} f_{32}}{\Delta\nu} \quad (3)$$

where Δn_{32} is the 3-D inverted population density, $f_{32} = (4\pi m^* \nu_{32} z_{32}^2)/\hbar$ is the unitless oscillator strength, z_{32} is the dipole-matrix element for the radiative transition, m^* is the conduction band effective mass, and n_{r} is the refractive index of the material. At the design bias corresponding to the $1'$–3 alignment, for a module length L_{mod}, the population-inversion density can be written using rate equations as

$$\Delta n_{32} = \frac{J_{1'3}}{e L_{\mathrm{mod}}} \tau_3 \left(1 - \frac{\tau_{21}}{\tau_{32}} \right). \quad (4)$$

A. Diagonal Resonant-Phonon Design for $\nu > 2$-THz QCLs

The aforementioned basic three-level QCL equations will now be used to describe the important design features of a *diagonal resonant-phonon* terahertz QCL design [22] that has shown the best temperature performance for any terahertz QCL to date. The design-bias conduction band diagram and experimental results in pulsed operation from a representative device are shown in Fig. 3. For terahertz QCLs, the injector barrier is typically kept thick, since the subbands are closely spaced in energy, which typically means that the quantity $4\,\Omega_{1'3}^2 \tau_{\|} \tau_3$ in (1) is less

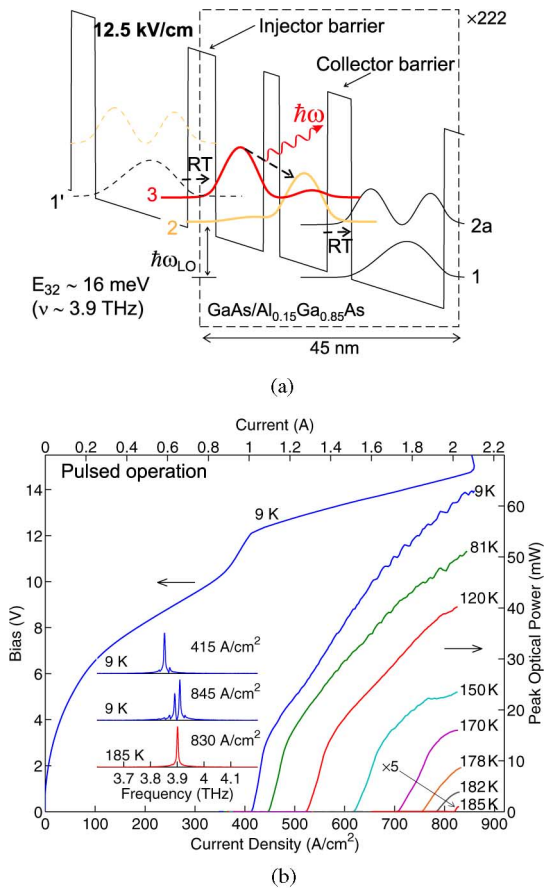

Fig. 3. (a) Design-bias conduction band diagram from a diagonal resonant-phonon design. The radiative transition is from $3 \rightarrow 2$. Depopulation of the lower laser subband 2 takes place by the mechanism of $2 \rightarrow 2a$ RT and $2a \rightarrow 1$ electron-LO-phonon scattering. Starting from the injector barrier, the layer thicknesses in nm are **4.8**/8.5/**2.8**/8.5/**4.2**/16.4 with the barriers indicated in bold fonts. The widest well is uniformly n-doped to obtain an effective 2-D density of 2.17×10^{10} cm^{-2} per period. (b) Experimental characteristics of a metal–metal ridge laser in pulsed operation. The device lased up to a heat-sink temperature of 185 K at a frequency of ~ 3.9 THz.

than or of the order of unity [46]. Hence, $J_{1'3}$ is a weak function of the upper subband lifetime τ_3 and is strongly dependent on the anticrossing energy $\hbar\Omega_{1'3}$ (or equivalently, the thickness of the injector barrier). Hence, designs that lead to a long upper subband lifetime achieve larger population inversion according to (4) without sacrificing the design-bias current density $J_{1'3}$ significantly. A design with a *diagonal* radiative transition (i.e., a small radiative oscillator strength f_{32}) achieves precisely that, since it keeps τ_{32} large, especially at higher temperatures when thermally activated LO-phonon scattering from $3 \rightarrow 2$ tends to diminish the population inversion [8]. The upper state lifetime decreases with temperature with an inverse exponential relation $\tau_{32} \propto \exp\left(\hbar\omega_{\mathrm{LO}} - E_{32}\right)/k_{\mathrm{B}}T_{\mathrm{e}}$, where T_{e} is the temperature of the 2-D electron gas in the upper subband. It was shown in [22] that the figure of merit $f_{32}\Delta n_{32}$ improves even as f_{32} decreases due to diagonality. An additional advantage for a diagonal design is the fact that the ratio $\Omega_{1'3}/\Omega_{1'2}$ improves with diagonality. For a given injector-barrier thickness, the parasitic leakage current density $J_{1'2}$ is, therefore, lowered leading to smaller threshold current densities. The 3.9-THz QCL design in Fig. 3(a) has the smallest oscillator strength of all earlier published terahertz QCLs while showing the record highest maximum operating temperature of $\sim$186 K for the best device from the grown wafer. Experimental characteristics from a high-power device is shown in Fig. 3(b), where 63 mW of peak optical power was measured from the single facet of an edge-emitting metal–metal waveguide ridge laser.

The merits of a *resonant-phonon* depopulation scheme [11], [47] are also worth noting in which RT plays an important role in the depopulation process as well. Comparing Fig. 3(a) to the three-level design of Fig. 2, the upper radiative subband is spatially separated from the injector subband in the case of resonant-phonon depopulation. The selectivity of $2 \rightarrow 2a$ RT ensures preferential depopulation of lower subband 2. Hence, a longer upper subband lifetime τ_{31} could be achieved, leading to large population inversion according to (4). A short lower subband lifetime could still be maintained in the resonant phonon scheme by keeping the *collector* barrier thin (i.e., the quantity $\hbar\Omega_{2,2a}$ large such that $2\Omega_{2,2a}^2\tau_{\|}\tau_{2a}$ is greater than unity), which maintains $\tau_{21} \sim \tau_{2a}$. Here, τ_{21} is an effective lifetime of the lower laser subband 2 such that the four-subband QCL in Fig. 3(a) could be analyzed with the three-level QCL equations by using the following expression [46]:

$$\tau_{21} = \tau_{2a}\left(\frac{2\Omega_{2,2a}^2\tau_{\|}\tau_{2a} + \Delta_{2,2a}^2\tau_{\|}^2 + 1}{2\Omega_{2,2a}^2\tau_{\|}\tau_{2a}}\right) \tag{5}$$

where, $\hbar\Delta_{2,2a} \equiv E_2 - E_{2a}$ is the energy detuning between subband 2 and $2a$ that is a function of the externally applied electrical bias.

B. $\nu < 2$-THz QCLs

It becomes increasingly difficult to realize QCLs operating below 2 THz. At low frequencies, the laser-level separation E_{ul} ($\sim$8 meV for $\nu \sim 2$ THz) becomes similar to the typical energy broadening of the subbands (few millielectonvolts). Hence, it becomes difficult to selectively inject from $i \rightarrow u$, where i is the injector subband and u is the upper laser subband. A *one-well injector* scheme [14] was developed initially to achieve superior injection selectivity for the first realization of a QCL operating below 2 THz [14]. For low-frequency QCLs, the injector barrier is typically kept thick to limit the $i \rightarrow l$ leakage current, which, however, reduces the obtainable dynamic range in current for the laser, and consequently, its maximum operating temperature. The lowest frequency for a QCL based on a phonon-depopulation scheme is 1.45 THz ($\hbar\omega \sim 6.0$ meV). The design is similar to the three-level design in [19] (see Fig. 2), and is shown in Fig. 4(a). An additional well is added to the active region to realize larger oscillator strength f_{32} for a fixed injection anticrossing $2\hbar\Omega_{1'3}$. As can be seen from the experimental results from a representative device in Fig. 4(b), the dynamic range in lasing for current is very small, which, therefore, limits the maximum operating temperature to a relatively small value of 37 K. A better temperature performance for the $\nu < 1.5$-THz QCLs is, however, obtained from a hybrid bound-to-continuum-based design scheme [48], where the separation between the lower laser subband and the injector subbands is

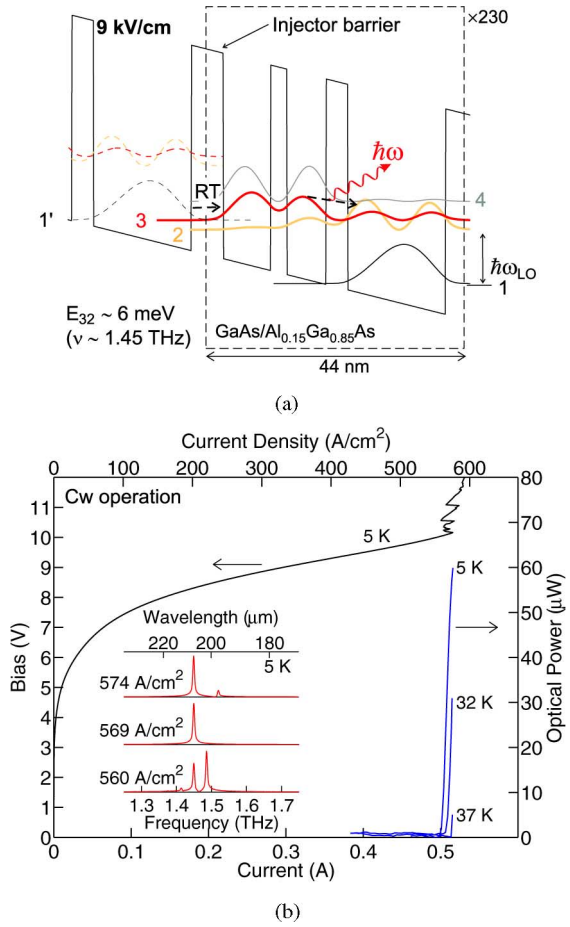

Fig. 4. (a) Design-bias conduction band diagram for a three-level intrawell-phonon QCL design for a radiative energy of 6 meV ($\nu \sim 1.45$ THz). The radiative transition is from $3 \rightarrow 2$. The lower laser subband 2 is depopulated directly by fast electron-LO-phonon scattering [19]. Starting from the injector barrier, the layer thicknesses in nm are **5.4**/8.2/**2.8**/6.8/**3.8**/17.0 with the barriers indicated in bold fonts. The widest well is uniformly n-doped to obtain an effective 2-D density of 2.7×10^{10} cm^{-2} per period. The injection anticrossing $2\hbar\Omega_{1'3} \sim 1.0$ meV, and the radiative oscillator strength is $f_{32} \sim 0.55$ at the design bias. An upper parasitic subband 4 exists in the active region with an energy separation of $E_{43} \sim 12.0$ meV; however, its contribution to electronic transport at low temperatures is expected to be negligible. (b) Experimental characteristics of a metal–metal ridge laser in CW operation. The device lased up to a heat-sink temperature of 37 K at $\nu \sim 1.45$ THz.

kept below the LO-phonon energy, which limits the parasitic leakage current density and leads to a greater dynamic range in lasing for current. A 1.2-THz QCL with $T_{\max} \sim 69$ K was realized in [48], which is currently the lowest operating frequency for QCLs without the assistance of an external magnetic field.

A wide variety of terahertz QCL designs have been reported in literature. However, all the earlier published terahertz QCLs relied on a RT injection scheme to populate the upper laser subband for which the maximum temperature of operation $T_{\max}$ has been empirically limited to a value $\sim \hbar\omega/k_{\rm B}$ across different designs and operating frequencies as shown by the shaded region in Fig. 5(a). This has led to a growing skepticism that room temperature operation of a terahertz QCL might never be possible. However, we recently surpassed this *empirical* limitation with a new *scattering-assisted* (SA) injection mechanism to achieve high-temperature operation even for the low-frequency designs, whereby a 1.8-THz QCL operating up to a value of $T_{\max} \sim 163$ K $\sim 1.9\ \hbar\omega/k_{\rm B}$ was realized [20]. The design scheme and the corresponding high-temperature experimental results are shown in Fig. 5(b) and (c), respectively.

The new terahertz QCL design in Fig. 5, in addition to being useful for applications in security-based imaging and astronomy, where $\nu \sim$1–2-THz radiation sources are highly desired, might pave the way for obtaining the much desired thermoelectrically cooled operation of a terahertz QCL. The improved temperature performance of the SA injection scheme could be understood from the following argument. For RT injection schemes, the injector barrier is typically kept thick to limit $i \rightarrow l$ leakage current, which reduces the obtainable dynamic range in current for the laser, and consequently, its maximum operating temperature [14], [48]. However, in the SA injection scheme, the cascade structure is designed to maximize current flow at a bias much higher than that for the *i–u* alignment. Consequently, potential barriers need not be made very thick to limit current flow that directly determines the amount of population inversion that could be established. This also results in greater optical power output for the laser. Whereas the peak optical power from all earlier $\nu < 2$-THz QCLs was $\leq$0.5 mW at 10 K [14], [15], [48], 28 mW of peak optical-power was detected from the 1.8-THz QCL of Fig. 5(c) at 10 K, and still $>$0.5 mW was detected at 160 K as shown. It may be noted that the operating current density in phonon-depopulated terahertz QCLs can be large (for example, >1 kA/cm^2 in [37]) owing to the strong low-bias parasitic current channels [43].The laser in Fig. 5(c) similarly shows a large operating current density of $\sim$1.2 kA/cm^2 at 160 K, and the plateau in the *I–V* at $\sim$20 V represents the parasitic leakage current channel. However, reduction in the parasitic leakage current is likely with subsequent design modifications, as exemplified by the recent report of a diagonal terahertz QCL [22] that lowered the operating current densities by a factor of two when compared to a design with a vertical radiative transition.

III. Metal–Metal Waveguides for Terahertz QCLs

Dielectric waveguiding is not a feasible option to confine the long-wavelength terahertz radiation. Two different types of waveguides based on surface plasmon electromagnetic modes have been utilized for terahertz QCLs as shown in Fig. 6. The single-plasmon waveguide [5] confines the terahertz mode using a metal top layer and a thin heavily doped semiconductor layer at the bottom of the active region such that the real part of the layer's refractive index is negative, and it supports a surface-plasmon mode that exponentially decays in the low-loss semiinsulating substrate. Such a waveguide results in high-power output due to a favorable mode profile in the vertical dimension. The second type of waveguide is a metal–metal structure [21] that confines the mode between two metal plates just like microstrip transmission lines at microwave frequencies. While the metal–metal waveguides provide strong mode confinement and lower loss at terahertz frequencies resulting in significantly higher operating temperatures, their emission characteristics are poor owing to the subwavelength mode confinement in the vertical

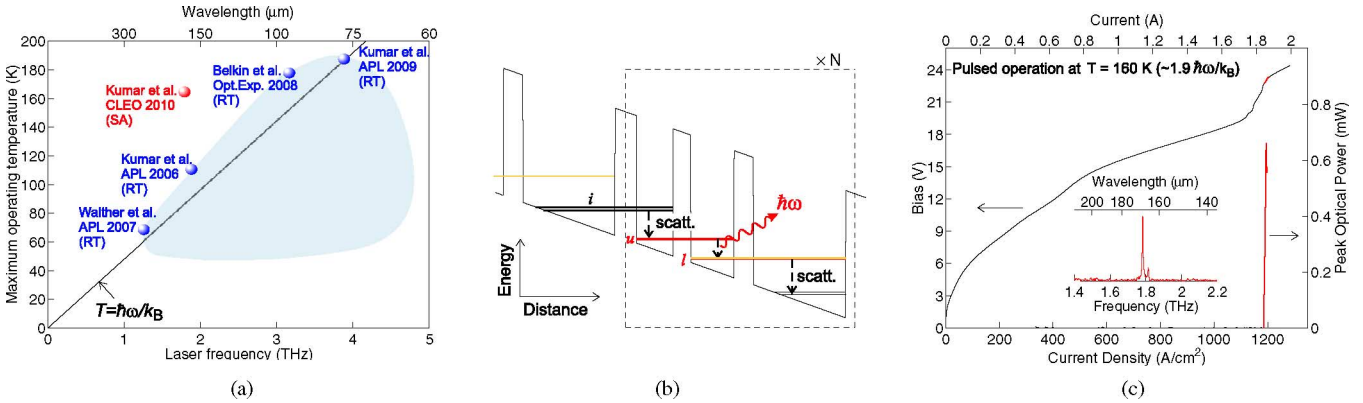

Fig. 5. (a) Survey of maximum operating temperatures for terahertz QCLs with respect to their operating frequency. A variety of designs have been published in literature spread across the shaded region [8]; however, the best performing designs in terms of highest operating temperatures are typically concentrated near the $T_{\max} \sim \hbar\omega/k_{\rm B}$ region. Till date, all of the earlier reported terahertz QCLs relied on a RT injection mechanism. (b) New SA injection design scheme for terahertz QCLs [20], where carriers are injected into the upper laser subband u by nonradiative scattering (primarily electron-LO-phonon scattering) from the injector subbands i. (c) Experimental behavior in pulsed operation from a 1.8-THz QCL with SA injection at a heat-sink temperature of 160 K. The device emit peak optical power of ~ 0.65 mW at 160 K, and lased up to $T_{\max} \sim 163$ K $\sim 1.9\hbar\omega/k_{\rm B}$ such that the carrier thermal energy is significantly larger than the photon energy in operation.

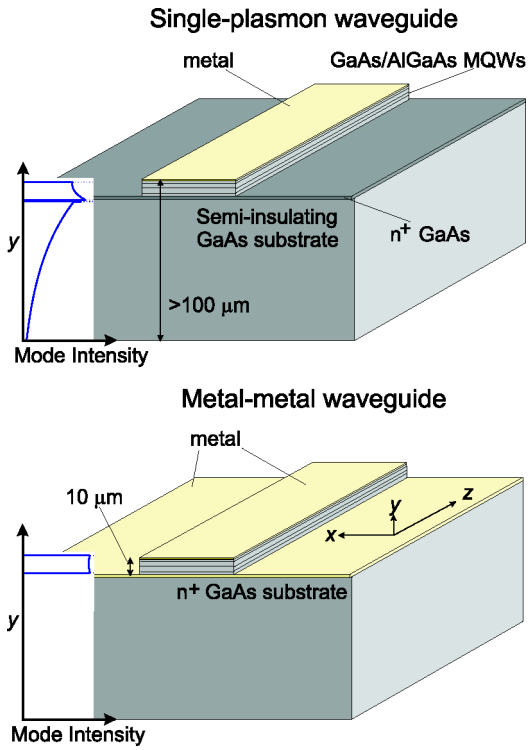

Fig. 6. Schematic diagrams of the two different type of waveguides for terahertz QCLs. Typical electromagnetic mode profiles in the vertical dimension are also plotted.

dimension, resulting in highly divergent beam patterns and low out-coupling of radiation [25], [26]. The aforementioned characteristics of the two types of waveguides are best exemplified by the following observation: a 4.2-THz QCL processed with the single-plasmon waveguide resulted in 248-mW peak optical power and a maximum operating temperature $T_{\max} \sim 105$ K, as reported in [50], the same wafer when processed with metal–metal waveguides resulted in an increased $T_{\max} \sim 165$ K, but a lower peak optical power of 26 mW as reported in [38].

Apart from their lower optical loss and the resulting higher temperature operation, metal–metal waveguides for terahertz QCLs offer several advantages owing to their ability to confine radiation in subwavelength scales even in the lateral dimensions. CW operation above liquid nitrogen temperature has been demonstrated by improving the flip-chip wafer bonding process required for fabricating such structures and by making the ridge devices narrow for efficient heat removal through the substrate [23], [24]. Ultralow threshold microcavity lasers with subwavelength optical volumes have also been realized [51]–[53]. However, from a usability perspective, the primary requirement has been the improvement of their emission characteristics to obtain narrow output beams with single-mode operation, and also develop techniques for continuous frequency tuning of the single-mode radiation. In the following, we describe some of our efforts toward the said objectives.

A. *Single-Mode Surface-Emitting Terahertz QCLs*

The electromagnetic mode intensity in the waveguide structures of Fig. 6 peaks locally at the interface between the semiconductor and the top metallic layer. Hence, having periodic discontinuity in that metallic layer (in the form of slits, for example) perturbs the mode strongly and is an efficient way to implement DFB in ridge waveguides. Metallic grating structures were implemented for the *single-plasmon* waveguides to obtain single-mode DFB operation in edge-emitting (first-order DFB) [54] as well as surface-emitting (second-order DFB) [55] configuration. However, implementation of a surface-emitting DFB structures turned out to be much more difficult in *metal-metal* terahertz QCLs, primarily because of the easy excitation of higher-order lateral modes and the large reflectivity from the end facets [25], both of which interfered with the desired DFB operation in such waveguides. Surface-emitting metal–metal DFB terahertz QCLs were particularly desired because of the potential for narrow beam patterns due to a much larger

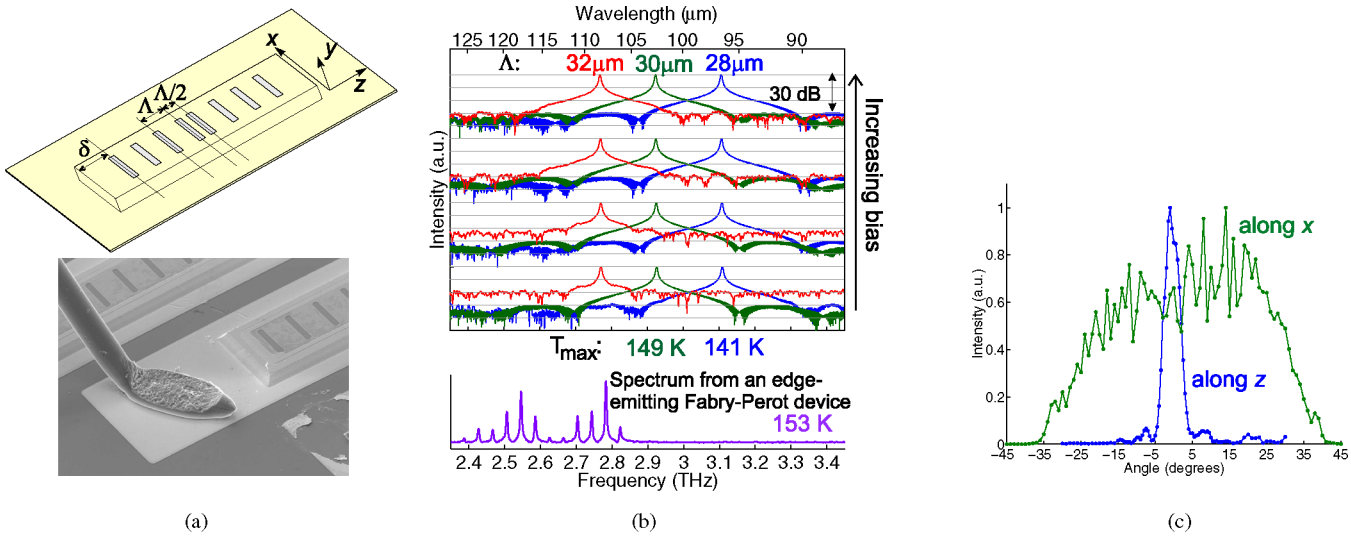

Fig. 7. (a) Surface-emitting second-order DFB-grating schematic for metal–metal terahertz QCLs [28]. An SEM picture of a fabricated device is also shown. (b) CW spectra from three surface-emitting DFB devices with different grating periods, measured as a function of increasing bias. Each device realized single-mode operation in all bias conditions. For comparison, emission spectrum from an edge-emitting ridge laser is also shown, which lased in multiple modes. The maximum operating temperatures in pulsed operation for different devices are also indicated alongside the spectra. (c) Far-field beam pattern of the $\Lambda = 30$-μm grating device. The beam pattern is narrow longitudinally, but broad in the transverse direction owing to the subwavelength dimension of the grating ridge in that direction.

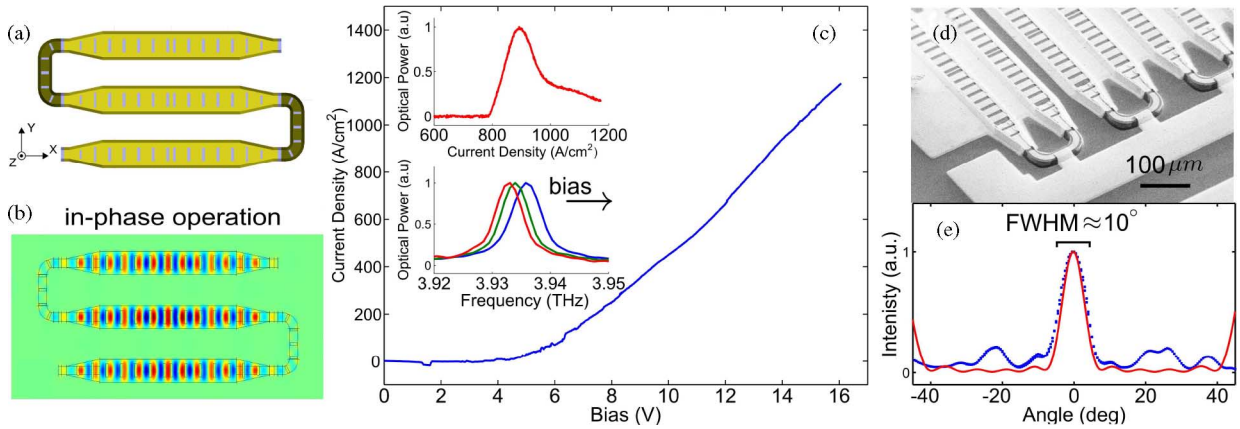

Fig. 8. (a) Schematic of a three-ridge THz QCL array for single-mode DFB operation to obtain narrow beam pattern in both the transverse and the longitudinal directions [49]. (b) Magnetic field inside the laser ridges for the desired "in-phase" mode from a 3-D full-wave finite-element method simulation. (c) Pulsed *I–V* curve of a six-ridge array at 10 K. Pulsed light-current curve and spectra at different bias are shown in the insets. The phase-locked array operated in a single mode, which could be tuned over a range of $\sim$1.5 GHz by separately biasing the electrically isolated portions of the "phase sectors." (d) SEM picture of a typical laser array that also shows the phase sectors at the longitudinal ends of the ridges, which could be biased separately to change the phase-locking condition marginally leading to a small electrical tuning of the DFB mode. (e) Measured (blue) and calculated (red) far-field "in-phase" beam pattern along the transverse direction from the six-ridge array. (Courtesy of Tsung-Yu Kao).

emitting area in that configuration, and also the possibility of larger optical power output for the same reason.

We achieved surface-emitting DFB operation in metal–metal terahertz QCLs with some unconventional design techniques. The designed grating structure and the corresponding experimental results are shown in Fig. 7. Due to subwavelength mode confinement in the vertical direction, there is a large mode mismatch at each grating step, which makes the DFB strongly coupled. Consequently, the conventional coupled mode theory cannot be applied for DFB design. Moreover, the mode behavior depends sensitively on the location of the facets due to their high reflectivities. To realize the desired DFB operation in such structures, a combination of techniques were implemented including precise control of phase of reflection at the facets, and use of metal on the sidewalls to eliminate higher order lateral modes [28]. Additionally, there was a relatively negligible penalty in the maximum operating temperature of the grating structures in comparison to the edge-emitting ridge devices, as indicated in Fig. 7(b), even as the emission and spectral characteristics of the grating devices were greatly improved.

The surface-emitting DFB structure of Fig. 7 leads to an asymmetric beam pattern that is narrow along the grating direction, but much broader in the transverse direction. Recently, a second-order DFB phase-locked laser array structure was implemented by coupling different DFB laser ridges through carefully designed "phase sectors" as shown in Fig. 8 [49]. Each laser ridge

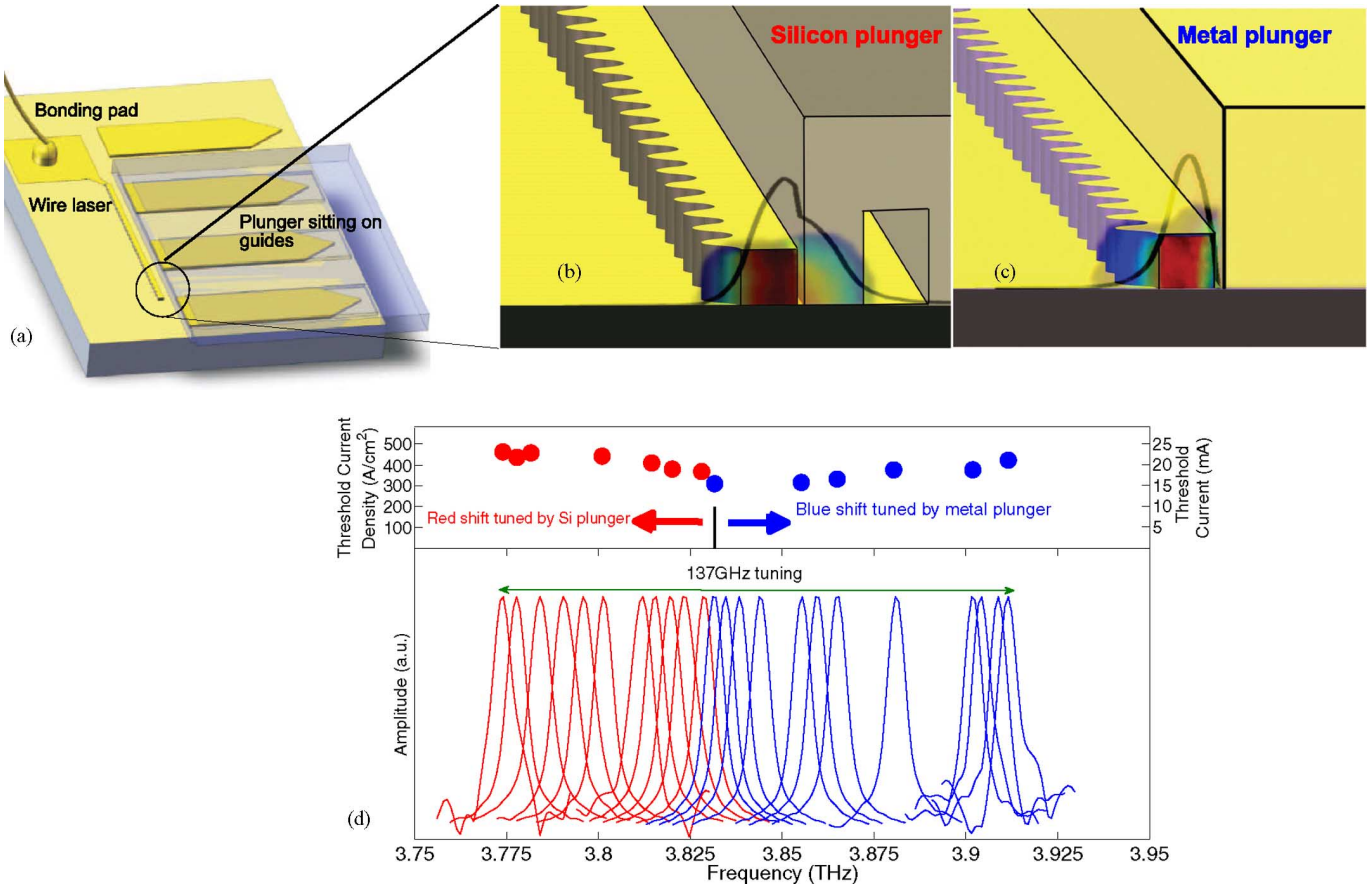

Fig. 9. (a) Schematic of device configuration for tuning a terahertz "wire-laser" [35]. (b) and (c) Illustration of the tuning mechanism with a silicon plunger and a metallic plunger respectively. The electrical field profile at the device facet is shown at the narrowest cross section of the DFB structure. DFB action to obtain single-mode operation is realized by a sideward corrugated first-order grating. The dark curve in the illustrations is the mode profile by integrating the electrical field component perpendicular to the ground plane. (d) Tuning results from a representative device. In the upper part, the threshold current densities of the device at different frequencies are plotted. The lower part shows broadband tuning of this device over a frequency range of 137 GHz.

is engineered to be locked "in-phase" with each other. The result is a 2-D phase-locked laser array with more symmetric beam patterns as shown in the figure. The phase in the individual ridges is locked with respect to each other due to the standing waves inside the phase sectors. The method can be considered as a "leaky wave" coupled scheme, which can be designed to preferentially excite the "in-phase" mode to realize a single-lobed beam pattern in the transverse dimension. Note that several other DFB techniques have recently been demonstrated to achieve symmetric beam patterns in 2-D, including 2-D photonic crystal structures [29], ring-cavity DFB lasers [56], [57] and edge-emitting third-order DFB structures [31]. However, an additional advantage of the phase-locking scheme of Fig. 8 is that it also provides a tuning mechanism for the DFB mode by changing the optical index of the semiconductor in the phase sectors, which can be induced by biasing the phase sectors separately that leads to a gain-induced change in the refractive index, as shown in Fig. 8(b). The fast and precise tuning ability can be useful in local oscillator applications for heterodyne spectroscopy techniques.

B. Tunable Terahertz QCLs

Tunable terahertz QCLs are highly desired for applications in sensing and spectroscopy. For these applications, mode-hop-free continuous tuning is required, which is usually achieved by using an external cavity grating. At terahertz frequencies, it is difficult to couple the beam diffracted from the grating back into the gain medium due to the long wavelengths associated with the terahertz frequencies compared to the subwavelength dimension of the emitting aperture [36]. The difficulty is further exacerbated by the required cryogenic operation. As a result, continuous frequency tuning using an external cavity grating has yet to be achieved. In addition, alternative electrical tuning by changing the refractive index due to temperature [28] or due to a cavity pulling effect [58] only produces a relatively small fractional tuning ($<1\%$).

Recently, we developed a novel tuning mechanism based on a unique "wire laser" device whose transverse dimension $w \ll l$ the length [35]. In a uniform gain medium, the lasing frequency for a particular resonant mode is determined by its $\omega - k$ dispersion relation $k_z^2 + k_\perp^2 = \omega^2 \mu\epsilon$, where k_z ($k_\perp$) is the component of the k-vector in the longitudinal (transverse) direction, ω is the frequency, $\mu = \mu_0$ is the vacuum permeability, and ϵ is the dielectric constant. The lasing frequency ω of an already fabricated device can be tuned by changing the values of k_z, $k_\perp$, or ϵ. Out of these three parameters, very little effort has been made to change $k_\perp$. This is because for most solid-state and semiconductor lasers, λ is comparable, or often smaller than the transverse

dimension of the cavity w. Consequently, little mode leaks out in the transverse directions and very little change can be made to $k_\perp$. However, terahertz QCLs based on metal–metal waveguides can be made with deep subwavelength widths, allowing manipulation of $k_\perp$. In [59], unexpected radiation patterns are attributed to a substantial fraction of the mode that travels outside of the wire laser. This unusual feature allows tuning of the lasing frequency by changing $k_\perp$, which is realized by moving either a dielectric or a metallic "plunger," close to the wire-laser, as shown in Fig. 9. If a dielectric plunger is used (silicon in this case), as it is pushed toward the laser, it extracts the mode from the gain medium, effectively expanding the mode profile in the transverse direction, as shown in Fig. 9(b). Consequently, the value of $k_\perp$ decreases and red-shift tuning is achieved. Similarly, if a metal plunger is used (gold in this case), $k_\perp$ increases as the plunger is pushed toward the laser as the mode approaches cutoff in the transverse dimension, which then results in blue-shift tuning.

Fig. 9 shows the schematic of the device design and the experimental results for a 3.8-THz QCL. In order to assure a continuous tuning of a single lasing mode, an asymmetric corrugation structure is used [60], with the flat side facing the plunger. The laser ridge had 12.5 μm average width, 3-μm sinusoidal grating modulation, 30 periods, and a grating period of $\Lambda = 13.7$ μm. In the same fabrication process that defined the DFB laser ridges, rails perpendicular to the laser ridges to guide the plungers were also fabricated. During operations, the plunger was pressed down and could only be pushed forward toward the laser ridge. A red-shift tuning of 57 GHz and a blue-shift tuning of 80 GHz was achieved as shown in Fig. 9(d) resulting in a combined tuning of 137 GHz, or 3.6% of the 3.8-THz center frequency. The threshold current density at different plunger positions is also plotted, which exhibits a moderate increase as either silicon or a metal plunger is pushed toward the laser ridge. Hence, a robust technique to realize continuous frequency tuning of a single-mode terahertz QCL has been demonstrated.

ACKNOWLEDGMENT

The author would like to thank colleagues whose work is represented in this review, namely, Q. Hu, J. L. Reno, B. S. Williams, H. Callebaut, A. W. M. Lee, Q. Qin, C. W. I. Chan, and T.-Y. Kao.

REFERENCES

[1] D. L. Woolard, E. R. Brown, M. Pepper, and M. Kemp, "Terahertz frequency sensing and imaging: A time of reckoning future applications?," *Proc. IEEE*, vol. 93, no. 10, pp. 1722–1743, Oct. 2005.

[2] P. H. Siegel, "Terahertz technology," *IEEE Trans. Microw. Theory Tech.*, vol. 50, no. 3, pp. 910–928, Mar. 2002.

[3] W. L. Chan, J. Diebel, and D. M. Mittleman, "Imaging with terahertz radiation," *Rep. Prog. Phys.*, vol. 70, pp. 1325–1379, 2007.

[4] P. H. Siegel, "Terahertz technology in biology and medicine," *IEEE Trans. Microwave Theory Tech.*, vol. 52, no. 10, pp. 2438–2447, Oct. 2004.

[5] R. Köhler, A. Tredicucci, F. Beltram, H. E. Beere, E. H. Linfield, A. G. Davies, D. A. Ritchie, R. C. Iotti, and F. Rossi, "Terahertz semiconductor-heterostructure laser," *Nature*, vol. 417, pp. 156–159, 2002.

[6] B. Ferguson and X.-C. Zhang, "Materials for terahertz science and technology," *Nature Mater.*, vol. 1, pp. 26–33, 2006.

[7] M. Tonouchi, "Cutting-edge terahertz technology," *Nature Photon.*, vol. 1, pp. 97–105, 2007.

[8] B. S. Williams, "Terahertz quantum-cascade lasers," *Nature Photon.*, vol. 1, pp. 517–525, 2007.

[9] S. Kumar and A. W. M. Lee, "Resonant-phonon terahertz quantum-cascade lasers and video-rate terahertz imaging," *IEEE J. Sel. Topics Quantum Electron.*, vol. 14, no. 2, pp. 333–344, Mar./Apr. 2008.

[10] G. Scalari, C. Walther, M. Fischer, R. Terazzi, H. Beere, D. Ritchie, and J. Faist, "THz and sub-THz quantum cascade lasers," *Laser Photon. Rev.*, vol. 3, pp. 45–105, 2009.

[11] B. S. Williams, H. Callebaut, S. Kumar, Q. Hu, and J. L. Reno, "3.4-THz quantum cascade laser based on longitudinal-optical-phonon scattering for depopulation," *Appl. Phys. Lett.*, vol. 82, pp. 1015–1017, 2003.

[12] G. Scalari, L. Ajili, J. Faist, H. Beere, E. Linfield, D. Ritchie, and G. Davies, "Far-infrared ($\lambda \cong 87$ μm) bound-to-continuum quantum- cascade lasers operating up to 90 K," *Appl. Phys. Lett.*, vol. 82, pp. 3165–3167, 2003.

[13] R. Köhler, A. Tredicucci, C. Mauro, F. Beltram, H. E. Beere, E. H. Linfield, A. G. Davies, and D. A. Ritchie, "Terahertz quantum-cascade lasers based on an interlaced photon-phonon cascade," *Appl. Phys. Lett.*, vol. 84, pp. 1266–1268, 2004.

[14] S. Kumar, B. S. Williams, Q. Hu, and J. L. Reno, "1.9 THz quantum-cascade lasers with one-well injector," *Appl. Phys. Lett.*, vol. 88, pp. 121123-1–121123-3, 2006.

[15] C. Walther, G. Scalari, J. Faist, H. Beere, and D. Ritchie, "Low frequency terahertz quantum cascade laser operating from 1.6 to 1.8 THz," *Appl. Phys. Lett.*, vol. 89, pp. 231121-1–231121-3, 2006.

[16] H. Luo, S. R. Laframboise, Z. R. Wasilewski, G. C. Aers, H. C. Liu, and J. C. Cao, "Terahertz quantum-cascade lasers based on a three-well active module," *Appl. Phys. Lett.*, vol. 90, pp. 041112-1–041112-3, 2007.

[17] G. Scalari, R. Terazzi, M. Giovannini, N. Hoyler, and J. Faist, "Population inversion by resonant tunneling in quantum wells," *Appl. Phys. Lett.*, vol. 91, pp. 032103-1–032103-3, 2007.

[18] G. Scalari, M. I. Amanti, M. Fischer, R. Terazzi, C. Walther, M. Beck, and J. Faist, "Step well quantum cascade laser emitting at 3 THz," *Appl. Phys. Lett.*, vol. 94, pp. 041114-1–041114-3, 2009.

[19] S. Kumar, C. W. I. Chan, Q. Hu, and J. L. Reno, "Two-well terahertz quantum-cascade laser with direct intrawell-phonon depopulation," *Appl. Phys. Lett.*, vol. 95, pp. 141110-1–141110-3, 2009.

[20] S. Kumar, C. W. I. Chan, Q. Hu, and J. L. Reno, "Operation of a 1.8-THz quantum-cascade laser above 160 K," presented at the Conf. Lasers Electro-Opt., San Jose, CA, May 16–21, 2010.

[21] B. S. Williams, S. Kumar, H. Callebaut, Q. Hu, and J. L. Reno, "Terahertz quantum-cascade laser at $\lambda \approx 100$ μm using metal waveguide for mode confinement," *Appl. Phys. Lett.*, vol. 83, pp. 2124–2127, 2003.

[22] S. Kumar, Q. Hu, and J. L. Reno, "186 K operation of terahertz quantum-cascade lasers based on a diagonal design," *Appl. Phys. Lett.*, vol. 94, pp. 131105-1–131105-3, 2009.

[23] S. Kumar, B. S. Williams, S. Kohen, Q. Hu, and J. L. Reno, "Continuous-wave operation of terahertz quantum-cascade lasers above liquid-nitrogen temperature," *Appl. Phys. Lett.*, vol. 84, pp. 2494–2497, 2004.

[24] B. S. Williams, S. Kumar, Q. Hu, and J. L. Reno, "Operation of terahertz quantum-cascade lasers at 164 K in pulsed mode and at 117 K in continuous-wave mode," *Opt. Exp.*, vol. 13, pp. 3331–3339, 2005.

[25] S. Kohen, B. S. Williams, and Q. Hu, "Electromagnetic modeling of terahertz quantum cascade laser waveguides and resonators," *J. Appl. Phys.*, vol. 97, pp. 053106-1–053106-9, 2005.

[26] A. J. L. Adam, I. Kašalynas, J. N. Hovenier, T. O. Klaassen, J. R. Gao, E. E. Orlova, B. S. Williams, S. Kumar, Q. Hu, and J. L. Reno, "Beam patterns of terahertz quantum cascade lasers with subwavelength cavity dimensions," *Appl. Phys. Lett.*, vol. 88, pp. 151105-1–151105-3, 2006.

[27] J. A. Fan, M. A. Belkin, F. Capasso, S. Khanna, M. Lachab, A. G. Davies, and E. H. Linfield, "Surface emitting terahertz quantum cascade laser with a double-metal waveguide," *Opt. Exp.*, vol. 14, pp. 11672–11680, 2007.

[28] S. Kumar, B. S. Williams, Q. Qin, A. W. M. Lee, Q. Hu, and J. L. Reno, "Surface-emitting distributed feedback terahertz quantum-cascade lasers in metal-metal waveguides," *Opt. Exp.*, vol. 15, pp. 113–128, 2007.

[29] Y. Chassagneux, R. Colombelli, W. Maineult, S. Barbieri, H. E. Beere, D. A. Ritchie, S. P. Khanna, E. H. Linfield, and A. G. Davies, "Electrically pumped photonic-crystal terahertz lasers controlled by boundary conditions," *Nature*, vol. 457, pp. 174–178, 2009.

[30] L. Mahler, A. Tredicucci, F. Beltram, C. Walther, J. Faist, B. Witzigmann, H. E. Beere, and D. A. Ritchie, "Vertically emitting microdisk lasers," *Nature Photon.*, vol. 3, pp. 46–49, 2009.

[31] M. I. Amanti, M. Fischer, G. Scalari, M. Beck, and J. Faist, "Low-divergence single-mode terahertz quantum cascade laser," *Nature Photon.*, vol. 3, pp. 586–590, 2009.
[32] A. W. M. Lee, Q. Qin, S. Kumar, B. S. Williams, Q. Hu, and J. L. Reno, "Real-time terahertz imaging over a standoff distance (> 25 m),". (2011). *Appl. Phys. Lett.*, vol. 89, pp. 141125-1–141125-3, 2006, 2011.
[33] D. Rabanus, U. U. Graf, M. Philipp, O. Ricken, J. Stutzki, B. Vowinkel, M. C. Wiedner, C. Walther, M. Fischer, and J. Faist, "Phase locking of a 1.5 terahertz quantum cascade laser and use as a local oscillator in a heterodyne HEB receiver," *Opt. Exp.*, vol. 17, pp. 1159–1168, 2009.
[34] P. Khosropanah, A. Baryshev, W. Zhang, W. Jellema, J. N. Hovenier, J. R. Gao, T. M. Klapwijk, D. G. Paveliev, B. S. Williams, S. Kumar, J. L. R. Q. Hu, B. Klein, and J. L. Hesler, "Phase locking of a 2.7 thz quantum cascade laser to a microwave reference," *Opt. Lett.*, vol. 34, pp. 2958–2960, 2009.
[35] Q. Qin, B. S. Williams, S. Kumar, Q. Hu, and J. L. Reno, "Tuning a terahertz wire laser," *Nature Photon.*, vol. 3, pp. 732–737, 2009.
[36] A. W. M. Lee, B. S. Williams, S. Kumar, Q. Hu, and J. L. Reno, "Tunable terahertz quantum cascade lasers with external gratings," *Opt. Lett.*, vol. 35, pp. 910–912, 2010.
[37] M. A. Belkin, J. A. Fan, S. Hormoz, F. Capasso, S. Khanna, M. Lachab, A. G. Davies, and E. H. Linfield, "Terahertz quantum cascade lasers with copper metal-metal waveguides operating up to 178 K," *Opt. Exp.*, vol. 16, pp. 3242–3248, 2008.
[38] A. W. M. Lee, Q. Qin, S. Kumar, B. S. Williams, Q. Hu, and J. L. Reno, "High-power and high-temperature THz quantum-cascade lasers based on lens-coupled metal-metal waveguides," *Opt. Lett.*, vol. 32, pp. 2840–2842, 2007.
[39] H. Callebaut and Q. Hu, "Importance of coherence for electron transport in terahertz quantum cascade lasers," *J. Appl. Phys.*, vol. 98, pp. 104505-1–104505-8, 2005.
[40] R. F. Kazarinov and R. A. Suris, "Possibility of the amplification of electromagnetic waves in a semiconductor with a superlattice," *Sov. Phys. Semicond.*, vol. 5, pp. 707–800, 1971.
[41] C. Sirtori, F. Capasso, J. Faist, A. L. Hutchinson, D. L. Sivco, and A. Y. Cho, "Resonant tunneling in quantum cascade lasers," *IEEE J. Quantum Electron.*, vol. 34, no. 9, pp. 1722–1729, Sep. 1998.
[42] S. Kumar. (2007, Apr.) "Development of terahertz quantum-cascade lasers," Ph.D. dissertation, Dept. Elect. Eng. Comput. Sci., Massachusetts Inst. Technol. [Online]. Available: http://dspace.mit.edu/handle/1721.1/40501
[43] H. Callebaut, S. Kumar, B. S. Williams, Q. Hu, and J. L. Reno, "Analysis of transport properties of terahertz quantum cascade lasers," *Appl. Phys. Lett.*, vol. 83, pp. 207–209, 2003.
[44] L. L. Bonilla and H. T. Grahn, "Non-linear dynamics of semiconductor superlattices," *Rep. Prog. Phys.*, vol. 68, pp. 577–683, 2005.
[45] J. Faist, F. Capasso, D. L. Sivco, C. Sirtori, A. L. Hutchinson, and A. Y. Cho, "Quantum cascade laser," *Science*, vol. 264, pp. 553–556, 1994.
[46] S. Kumar and Q. Hu, "Coherence of resonant-tunneling transport in terahertz quantum-cascade lasers," *Phys. Rev. B*, vol. 80, pp. 245316-1–245316-14, 2009.
[47] Q. Hu, B. S. Williams, S. Kumar, H. Callebaut, S. Kohen, and J. L. Reno, "Resonant-phonon-assisted THz quantum-cascade lasers with metal-metal waveguides," *Semicond. Sci. Technol.*, vol. 20, pp. S228–S236, 2005.
[48] C. Walther, M. Fischer, G. Scalari, R. Terazzi, N. Hoyler, and J. Faist, "Quantum cascade lasers operating from 1.2 to 1.6 THz," *Appl. Phys. Lett.*, vol. 91, pp. 131122-1–131122-3, 2007.
[49] T.-Y. Kao, Q. Hu, and J. L. Reno, "Phase-locked arrays of surface-emitting terahertz quantum-cascade lasers," *Appl. Phys. Lett.*, vol. 96, pp. 101106-1–101106-3, 2010.
[50] B. S. Williams, S. Kumar, Q. Hu, and J. L. Reno, "High-power terahertz quantum-cascade lasers," *Electron. Lett.*, vol. 42, pp. 89–91, 2006.
[51] Y. Chassagneux, J. Palomo, R. Colombelli, S. Dhillon, C. Sirtori, H. Beere, J. Alton, and D. Ritchie, "Terahertz microcavity lasers with subwavelength mode volumes and thresholds in the milliampere range," *Appl. Phys. Lett.*, vol. 90, pp. 091113-1–091113-3, 2007.
[52] L. A. Dunbar, R. Houdré, G. Scalari, L. Sirigu, M. Giovannini, and J. Faist, "Small optical volume terahertz emitting microdisk quantum cascade lasers," *Appl. Phys. Lett.*, vol. 90, pp. 141114-1–141114-3, 2007.
[53] C. Walther, G. Scalari, M. I. Amanti, M. Beck, and J. Faist, "Microcavity laser oscillating in a circuit-based resonator," *Science*, vol. 327, pp. 1495–1497, 2010.
[54] L. Mahler, A. Tredicucci, R. Köhler, F. Beltram, H. E. Beere, E. H. Linfield, D. A. Ritchie, and A. G. Davies, "High-performance operation of single-mode terahertz quantum cascade lasers with metallic gratings," *Appl. Phys. Lett.*, vol. 87, pp. 181101-1–181101-3, 2005.
[55] O. Demichel, L. Mahler, T. Losco, C. Mauro, R. Green, A. Tredicucci, J. Xu, F. Beltram, H. E. Beere, D. A. Ritchie, and V. Tamošiūnas, "Surface plasmon photonic structures in terahertz quantum cascade lasers," *Opt. Exp.*, vol. 14, pp. 5335–5345, 2006.
[56] L. Mahler, M. I. Amanti, C. Walther, A. Tredicucci, F. Beltram, J. Faist, H. E. Beere, and D. A. Ritchie, "Distributed feedback ring resonators for vertically emitting terahertz quantum cascade lasers," *Opt. Exp.*, vol. 17, pp. 13031–13039, 2009.
[57] E. Mujagić, C. Deutsch, H. Detz, P. Klang, M. Nobile, A. M. Andrews, W. Schrenk, K. Unterrainer, and G. Strasser, "Vertically emitting terahertz quantum cascade ring lasers," *Appl. Phys. Lett.*, vol. 95, pp. 011120-1–011120-3, 2009.
[58] H. Zhang, L. A. Dunbar, G. Scalari, R. Houdre, and J. Faist, "Terahertz photonic crystal quantum cascade lasers," *Opt. Exp.*, vol. 15, pp. 16818–16827, 2007.
[59] E. E. Orlova, J. N. Hovenier, T. O. Klaassen, I. Kašalynas, A. J. L. Adam, J. R. Gao, T. M. Klapwijk, B. S. Williams, S. Kumar, Q. Hu, and J. L. Reno, "Antenna model for wire lasers," *Phys. Rev. Lett.*, vol. 96, pp. 173904-1–173904-4, 2006.
[60] B. S. Williams, S. Kumar, Q. Hu, and J. L. Reno, "Distributed-feedback terahertz quantum-cascade lasers with laterally corrugated metal waveguides," *Opt. Lett.*, vol. 30, pp. 2909–2911, 2005.

Sushil Kumar was born in Jaipur, India. He received the B.E. degree from the Delhi College of Engineering, Delhi, India, in 1998, the M.S. degree from the University of Michigan, Ann Arbor, in 2001, and the Ph.D. degree from the Massachusetts Institute of Technology, Cambridge, in 2007, all in the field of electrical engineering. His Ph.D. thesis focused on various aspects of the development of terahertz quantum cascade lasers (QCLs).

He is currently a Postdoctoral Associate at the Research Laboratory of Electronics, Massachusetts Institute of Technology, Cambridge. His research interests include development of terahertz QCLs and other devices based on intersubband transitions in semiconductor superlattices.